

# Improved technology of frequency-selective UHF electromagnetic shields containing helical elements

Olga V. Boiprav<sup>1</sup>, Natalia V. Bogush<sup>1</sup>

*1 Belarusian State University of Informatics and Radioelectronics, 6 P. Brovki Str., Minsk 220013 Republic of Belarus*

Corresponding author: Olga V. Boiprav (smu@bsuir.by)

Received 9 November 2022 ♦ Accepted 7 December 2022 ♦ Published 19 December 2022

**Citation:** Boiprav OV, Bogush NV (2022) Improved technology of frequency-selective UHF electromagnetic shields containing helical elements. *Modern Electronic Materials* 8(4): 157–164. <https://doi.org/10.3897/j.moem.8.4.100653>

## Abstract

An improved technology of frequency-selective electromagnetic shields has been considered. The technology has been improved by embedding classic Archimedean helical elements made from foiled materials into the bulk of the shields for the improvement of the frequency-selective performance of the shields and pinning of these elements in the bulk of the shields by means of fusion bonding. These design features provide for the main advantage of the improved technology in comparison with counterparts, i.e., lower time consumption. The technology has been improved in the following two aspects: 1) identification of helical element parameters providing for the greatest energy loss of the UHF electromagnetic radiation interacting with the helical elements; 2) identification of the optimum helical element arrangement in the shield bulk providing for the smallest transmission and reflection coefficient of the UHF electromagnetic radiation by the shields. Technology improvement in accordance with the former of the above aspects has been achieved based on analysis of publications dealing with mathematical simulation and study of the parameters of UHF electromagnetic radiation transmission by planar helical antennas. Technology improvement in accordance with the latter aspect has been achieved based on experimental data. Test shields have been fabricated with specifically arranged embedded helical elements, and comparison has been made between the UHF electromagnetic radiation transmission and reflection coefficients of the shields. Shields fabricated in accordance with the improved technology suggested herein show good promise for the electromagnetic noise protection of electronic devices.

## Keywords

aluminum foil, improved technology, frequency-selective electromagnetic shield

## 1. Introduction

The main application domains of frequency-selective UHF electromagnetic shields are currently the following:

- development of radio measuring devices (reference specimens are made on the basis of frequency-selective electromagnetic shields [1, 2]);
- electronic device protection against noise with exactly known frequencies [3–8].

Frequency-selective UHF electromagnetic shields can be fabricated using the following technologies:

1. Cutting out or punching of electrically conducting substrates to produce equally spaced openings (slots) having similar shapes and sizes [9, 10].
2. Ordered arrangement and pinning of elements made from electrically conducting materials and having specific (typically, similar) shapes and sizes in the dielectric matrix bulk [11–13]. Those elements are typically fabricated by milling, laser cutting or water-jet cutting [14].

3. 3D printing of metal-containing composite material elements having specific (typically, similar) shapes and sizes on the surface of dielectric substrates [15, 16].

Shields fabricated in accordance with the former of the above technologies are conventionally referred to as slot shields whereas those fabricated in accordance with the second or third technologies are known as wire shields [17].

Wire shields are currently fabricated and used more widely than slot shields as can be seen from the large scope of works published over the recent five years dealing with the development of technologies and study of properties of such shields in comparison with the scope of publications dealing with slot electromagnetic shields. Most likely the greater fabrication volume and wider application of wire shields in comparison with slot shields are caused by their lower cost. One should however bear in mind that wire shield technologies are typically more time-consuming than slot shield technologies because wire shield technologies include an extra stage of shaping and/or solidification of dielectric matrices.

Elements used for the fabrication of frequency-selective electromagnetic wire shields may have the following shapes: rod, triangle, circle, square, rectangle or cross [18–23]. It was reported [24] that the use of elements in the form of helical antennas shows good promise for the fabrication of frequency-selective shields. Results of the development and study of frequency-selective electromagnetic wire shields containing Fermat helical elements (a specific type of Archimedean helical elements) were published [25].

This work is targeted at the improvement of the general technology of frequency-selective electromagnetic wire shields and continuation of earlier reported studies [24, 25].

More specifically, the aim of this work is to improve the general technology of frequency-selective UHF electromagnetic shields containing classical Archimedean helical elements. The technology should be improved by reducing the time consumption of the overall process.

The following tasks had to be solved for achieving the aim of this work:

- choosing the parameters of helical elements for frequency-selective UHF electromagnetic shields;
- choosing auxiliary materials and equipment required for the implementation of the improved technology;
- documenting the improved technology of frequency-selective UHF electromagnetic shields with embedded helical elements;
- fabrication, in accordance with the documented improved technology, of laboratory specimens of frequency-selective UHF electromagnetic shields with embedded helical elements differing in the arrangement of said helical elements;
- measurement and comparison of UHF electromagnetic transmission and reflection coefficients of the test specimens.

## 2. Experimental

For the solution of the former task within the achievement of the overall aim of this work, data on the parameters of Archimedean helical antennas reported earlier [26] were used. Those results suggest that the greatest UHF electromagnetic radiation energy loss in such antennas occurs if the following conditions are satisfied [26]:

- the length of the smallest spiral turn is proportional to and comparable with the electromagnetic radiation wavelength (the minimum electromagnetic radiation wavelength) at the working frequency (in the working frequency range) of the antenna;
- the number of helical turns is 2;
- the thickness  $W$  of the conductor the antenna is made from and the helical turn spacing  $S$  (Fig. 1) are in the following ratio:

$$\frac{W}{W + S} = 0,167.$$

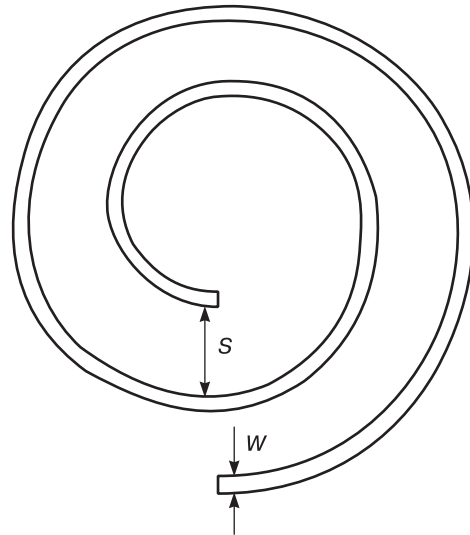


**Figure 1.** Schematic of a spiral element:  $S$  is the helical turn spacing;  $W$  is the conductor thickness

For the solution of the second task it was suggested to use synthetic unwoven fabric as the dielectric matrix (i.e. an auxiliary material) for the fabrication of frequency-selective electromagnetic wire shields. The helical elements made from electrically conducting materials and having similar shapes and sizes were pinned in the bulk of the dielectric matrix by fusion bonding at a temperature exceeding the melting point of the synthetic unwoven fabric ( $\sim 250$  °C) and the melting point of the material said helical elements are made from.

Upon the results of solving the third task the improved technology of frequency-selective UHF electromagnetic shields containing helical elements was documented. The technology includes the following stages.

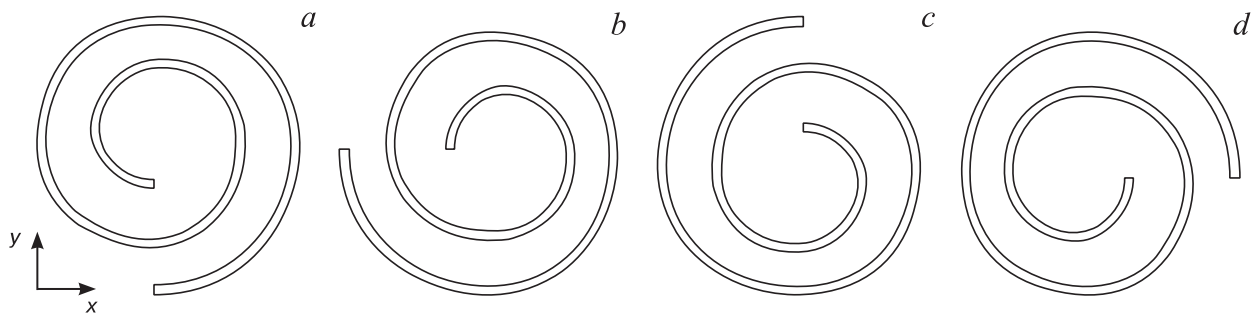


**Figure 2.** Schematic of helical element embedded in the bulk of specimens (a) I, (b) II, (c) III and (d) IV

*Stage 1.* Cutting a roll of radio-transparent synthetic unwoven fiber fabric into similar fragments subject to the following conditions:

- the shapes and sizes of the fragments are similar to the shapes and sizes of the electromagnetic shields to be fabricated;
- the number of the fragments is twice the number of the electromagnetic shields to be fabricated.

*Stage 2.* Fabrication of helical elements from electrically conducting materials subject to the conditions identified during the solution of the former tasks.

*Stage 3.* Arrangement of the fabricated helical elements on the surfaces of synthetic unwoven fabric fragments subject to the following conditions:

- half of the synthetic unwoven fabric fragments fabricated as a result of Stage 1 are used;
- the helical elements are arranged at a spacing exceeding the electromagnetic radiation wavelength (the minimum electromagnetic radiation wavelength) at the working frequency (in the working frequency range) of the electromagnetic shields to be fabricated.

*Stage 4.* Arrangement of the surface of each fragment fabricated as a result of Stage 3 on one fragment fabricated as a result of Stage 1.

*Stage 5.* Fusion bonding of the structures fabricated as a result of Stages 1–4 under the conditions identified as a result of the solution of the second task within the aim of this work.

Upon the results of solving the fourth task within the aim of this work in accordance with the improved technology, four types (I–IV) of test specimens of frequency-selective UHF electromagnetic shields were fabricated. The test specimens of each type differed in the arrangement of the helical elements embedded in the bulk of the shields. The helical elements embedded in the bulk of I type specimens were arranged relative to the electromagnetic radiation propagation front in the  $XOY$  plane as shown in Fig. 2 a, whereas the helical elements embedded in the bulk of II, III and IV type specimens were arranged as shown in Fig. 2 b–d, respectively.

For solving the task of experimental verification of the improved technology developed herein, the following parameters of helical elements for frequency-selective UHF electromagnetic shields were chosen: the smallest helical turn length was 4.7 cm, its radius  $R_1$  was 0.75 cm, the spiral radius was 2.25 cm,  $W = 0.3$  cm and  $S = 1.5$  cm. The helical elements were made under laboratory conditions from ribbon-shaped aluminum foil fragments. Each of the fragments was formed in cavities of specially designed template wafers the shape of which replicated the shape of the Archimedean spiral.

Aluminum foil was chosen for the fabrication of helical elements due to its high flexibility in comparison with other sheet metal-containing materials or wire-shaped metal-containing materials. This advantage of aluminum foil reduces the time consumption for the fabrication of aluminum foil helical elements using template wafers under laboratory conditions in comparison with that for the fabrication of similar elements from other abovementioned metal-containing materials.

Figure 3 shows the appearance of a fabricated helical element.

Figure 4 shows appearance of a surface fragment of the I type specimen.

The electromagnetic transmission and reflection coefficients of the specimens were measured on an



**Figure 3.** Appearance of helical element embedded in the bulk of I type specimen

instrument that contained the following metering devices: a SNA0.01-18 transmission and reflection coefficient analyzer, coaxial waveguides, two P6-23M horn antennas and a short-circuit switch. For electromagnetic transmission coefficient measurements, all these devices were used except the short-circuit switch, whereas for electromagnetic reflection coefficient measurements, all these devices were used except one horn antenna.

Before transmission and reflection coefficient measurements the instrument was calibrated in order to evaluate the effect of electromagnetic wave attenuation in the antenna circuit and coaxial waveguides of the measuring instrument on the parameter readings.

For instrument calibration before specimen electromagnetic transmission coefficient measurements the transmitting and receiving antennas connected to the SNA 0.01-18 reflection and transmission coefficient analyzer were installed in front of each other.

For instrument calibration before specimen electromagnetic reflection coefficient measurements the short-circuit switch in the form of a flat copper plate was installed before the transmitting antenna connected to the SNA 0.01-18 reflection and transmission coefficient analyzer.

Specimen electromagnetic reflection coefficient measurements were run in short-circuit mode (the specimen was connected between the transmitting antenna and the flat copper short-circuit switching plate). Results of these measurements are typically used in practice for assessing the performance of shields in the reduction of passive electromagnetic noise caused by the reflection of electromagnetic waves generated by electronic devices from metallic objects and subsequent redirection of electromagnetic waves to the device locations. Passive noise can impact the performance of electronic devices to almost the same extent as active noise (i.e., noise generated by sources in the vicinity of electronic devices).

The size of each test specimen was chosen to be  $30 \times 40 \text{ cm}^2$  taking into account the dimensions of the antenna flanges of the measuring instrument used for specimen electromagnetic reflection and transmission coefficient measurements.

Electromagnetic reflection and transmission coefficient measurements were run in the 0.7–3.0 GHz range because the helical turn lengths of the helical elements embedded in the bulk of the specimens fabricated in accordance with the improved technology were comparable with the electromagnetic radiation wavelengths for this frequency range.

### 3. Results and discussion

Figure 5 shows 0.7–3.0 GHz frequency responses of electromagnetic transmission coefficient of the specimens fabricated in accordance with the improved technology.

It can be seen that the 0.7–3.0 GHz frequency response of the electromagnetic transmission coefficient for the I

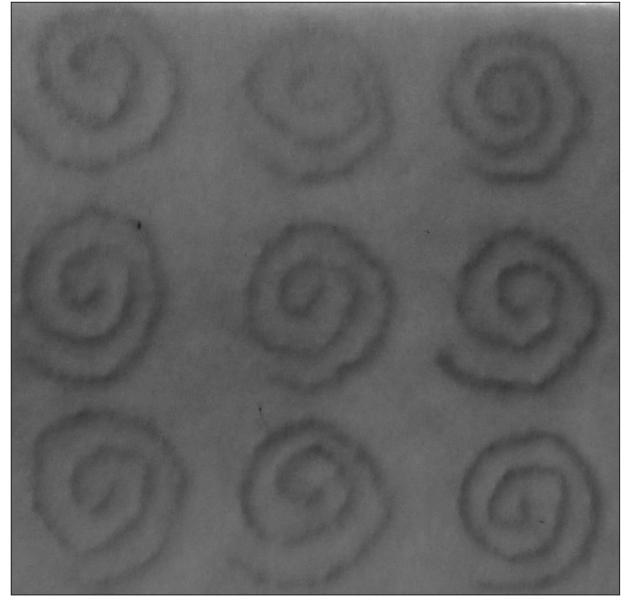


Figure 4. Appearance of surface fragment of I type specimen

type specimen is almost identical to that for the III type specimen. This is caused by the fact that electromagnetic waves interacting with the I type specimen and intersecting its surface at the points  $y_1, y_2$  and  $y_3$  (Fig. 6 a) have the same phase as the electromagnetic waves interacting with the III type specimen and intersecting its surface at the points  $y_1^*, y_2^*$  and  $y_3^*$  (Fig. 6 b).

The same feature is inherent to the 0.7–3.0 GHz frequency response of electromagnetic transmission coefficients for II and IV type specimens. This is caused by the fact that electromagnetic waves interacting with the II type specimen and intersecting its surface at the points  $x_1, x_2$  and  $x_3$  (Fig., 6 c) have the same phase as the electromagnetic waves interacting with the IV type specimen and intersecting its surface at the points  $x_1^*, x_2^*$  and  $x_3^*$  (Fig. 6 d).

The electromagnetic transmission coefficient of the I and III type specimens in the 0.7–3.0 GHz range varies from  $-0.1$  to  $-0.7$  dB and that of the II and IV type specimens, from  $-0.1$  to  $-23.0$  dB. The lower electromagnetic transmission coefficients of the II and IV type specimens compared to those of the I and type III specimens are caused by the fact that the amplitudes of the electromagnetic waves interacting with the II and IV type specimens at the points  $x_1, x_2$  and  $x_3$  ( $x_1^*, x_2^*$  and  $x_3^*$ ) are lower than those of the electromagnetic waves interacting with the I and III specimens at the points  $y_1, y_2$  and  $y_3$  ( $y_1^*, y_2^*$  and  $y_3^*$ ). This in turn is caused by the phase shift between the electromagnetic waves at the points  $x_1, x_2$  and  $x_3$  ( $x_1^*, x_2^*$  and  $x_3^*$ ) and the points  $y_1, y_2$  and  $y_3$  ( $y_1^*, y_2^*$  and  $y_3^*$ ).

The frequency responses of the I and III type specimens feature two frequency bands: 1.1–1.3 GHz (resonance frequency 1.15 GHz) and 1.7–2.0 GHz (resonance frequency 1.8 GHz). This can be caused by the following:

- the electromagnetic radiation wavelengths for the abovementioned resonance frequencies are multiples of the distance from the centers of the helical elements

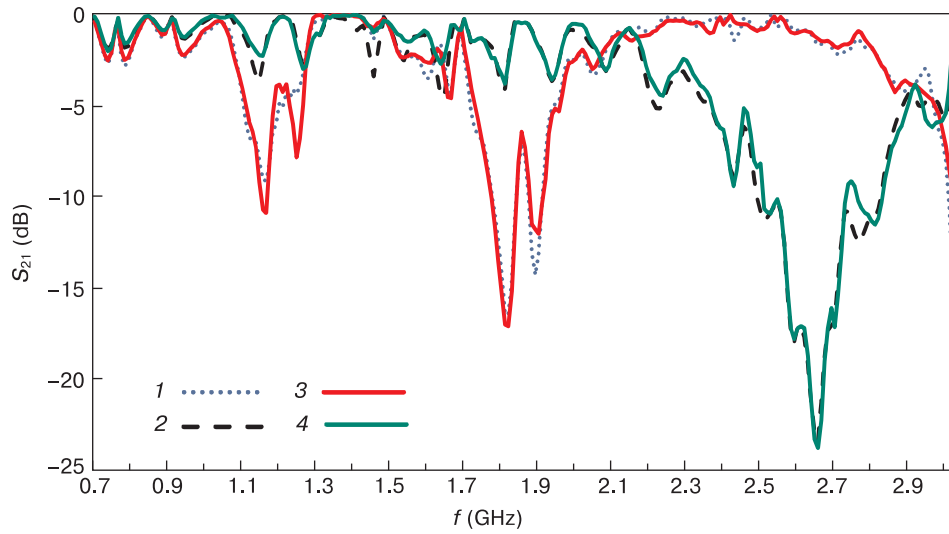


**Figure 5.** 0.7–3.0 GHz frequency response of electromagnetic transmission coefficient for I, II, III and IV type specimens (curves 1, 2, 3 and 4, respectively)

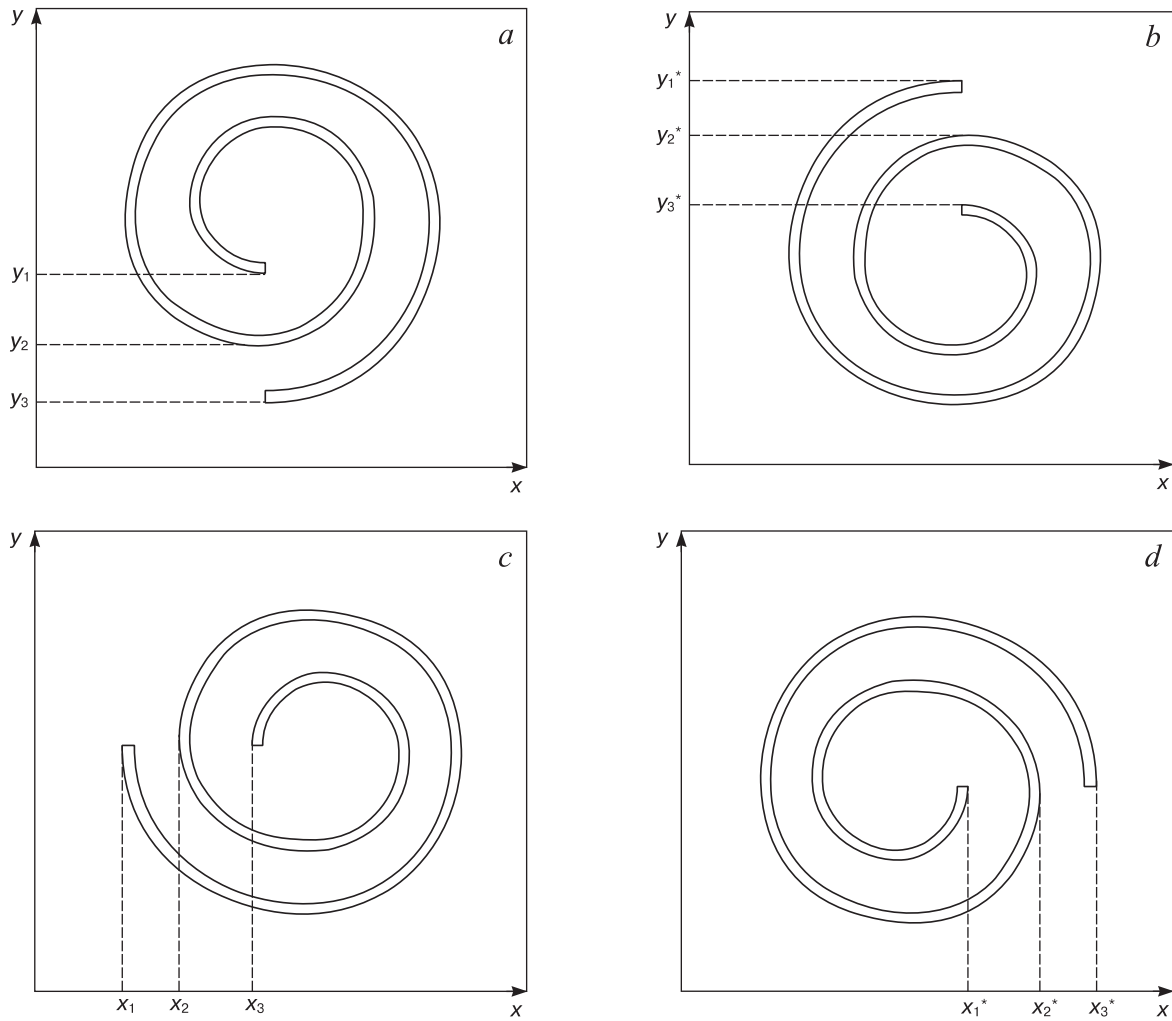


**Figure 6.** Locations and notations of the start and end points of helical element turns embedded in the bulk of (a) I, (b) III, (c) II and (d) IV type specimens

embedded in the bulk of the I and III type specimens to the points  $y_3 (y_3^*)$  and  $y_1 (y_1^*)$ , respectively;

– the amplitudes of the electromagnetic waves interacting with the I and III type specimens at the points  $y_3 (y_3^*)$  and  $y_1 (y_1^*)$  are the greatest.

The frequency responses of the II and IV type specimens feature one band, i.e., 2.3–3.0 GHz (resonance frequency 2.65 GHz). This can be caused by the following:

– the electromagnetic radiation wavelength for the abovementioned resonance frequency is a multiple of the distance from the centers of the helical elements embedded in the bulk of the II and IV type specimens to the points  $x_2 (x_2^*)$ ;

– the amplitude of the electromagnetic waves interacting with the I and III type specimens at the points  $x_3 (y_3^*)$  and  $x_1 (x_1^*)$  is the greatest.

Taking into account the above results it was concluded that the resonance frequencies  $f_{res}$  corresponding to the lowest electromagnetic transmission coefficient of the shields fabricated in accordance with the improved technology can be determined on the basis of the following relationships:

– if the helical elements embedded in the bulk of the shields are arranged as shown in Fig. 2 *a* and *c*, then

$$f_{resi} = \frac{S + R_1(i-1)}{8},$$

where  $i = \{0, 1\}$ ;

– if the helical elements embedded in the bulk of the shields are arranged as shown in Fig. 2 *b* and *d*, then

$$f_{res} = \frac{S + 2R_1}{8}.$$

It should be noted that the electromagnetic transmission coefficients of the shields fabricated in accordance with the improved technology are comparable to the electromagnetic transmission coefficients of the shields reported earlier [25] with Fermat helical elements

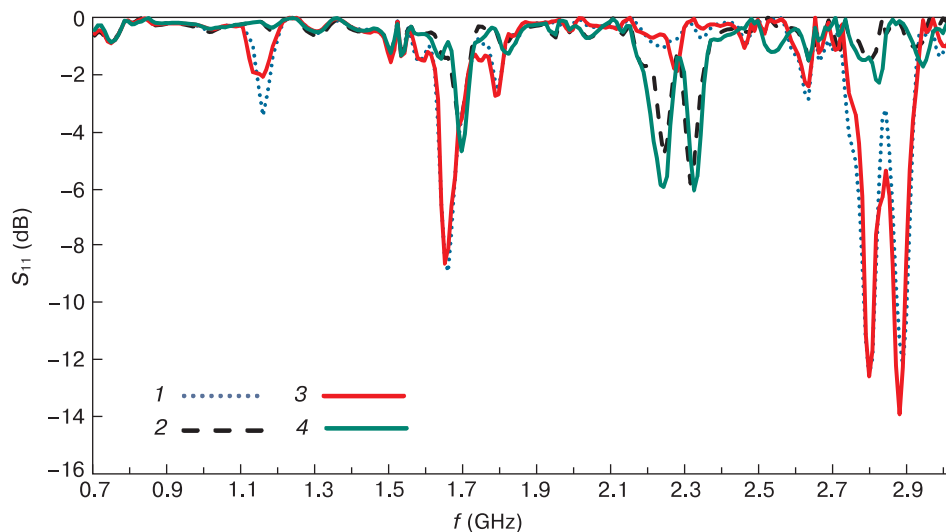
embedded in the bulk. One can therefore conclude that changing the type of helical elements (Fermat helical elements to Archimedean helical elements) embedded in the bulk of frequency-selective shields does not affect the performance of the shields in a critical manner. However, the fabrication of classical Archimedean helical elements is less time-consuming than the fabrication of Fermat helical elements.

Figure 7 shows 0.7–3.0 GHz frequency responses of the electromagnetic reflection coefficients for the specimens fabricated in accordance with the improved technology.

It can be seen from Fig. 7 that the 0.7–3.0 GHz frequency response of the electromagnetic reflection coefficients for the specimens fabricated in accordance with the improved technology is similar to that of the electromagnetic transmission coefficients for the specimens. The origins of this similarity are the same as those of the similarity between the frequency responses of the electromagnetic transmission coefficients for the specimens as discussed above.

The 0.7–3.0 GHz electromagnetic reflection coefficients of the I and III type specimens measured in short circuit mode vary from  $-0.1$  to  $-15.0$  dB and those of the II and IV type specimens, from  $-0.1$  to  $-6.0$  dB. The lower electromagnetic reflection coefficients of the I and III type specimens as compared to those of the II and IV type specimens can be caused by the following. The amplitude of the electromagnetic waves reflected by the metallic substrate used during the electromagnetic reflection coefficient measurements in short circuit mode and interacting with the I and III type specimens at the points  $x_1, x_2$  and  $x_3 (x_1^*, x_2^*$  and  $x_3^*)$  is greater than the amplitude of the respective electromagnetic waves interacting with the II and IV type specimens at the points  $y_1, y_2$  and  $y_3 (y_1^*, y_2^*$  and  $y_3^*)$ .

The frequency responses of electromagnetic reflection coefficients in question, by analogy with those of the



**Figure 7.** 0.7–3.0 GHz frequency response of electromagnetic reflection coefficients for I, II, III and IV type specimens (curves 1, 2, 3 and 4, respectively)

electromagnetic transmission coefficients (see Fig. 5), have a resonance pattern. The minima (i.e., the resonance frequencies) of the frequency responses of electromagnetic reflection coefficients for the I and III type specimens are at 1.15, 1.65, 1.8, 2.65, 2.75 and 2.85 GHz, and those for the II and IV type specimens are at 1.7, 2.25 and 2.35 GHz. The greater number of minima in these frequency responses as compared with those in the frequency responses of electromagnetic transmission coefficients for the test specimens is caused by the following:

- during short circuit mode measurements the reflected electromagnetic waves form as a result of a combination of incident electromagnetic waves reflected from specimen surfaces and electromagnetic waves having passed through the specimen bulk and reflected from the metallic substrate;

- at the measuring antenna, the phase of the electromagnetic waves reflected from the specimen surface is shifted relative to the phase of the electromagnetic waves reflected from the metallic substrate, the phase shift being determined by the frequency of the electromagnetic waves.

## 4. Conclusion

Changing the arrangement of helical elements embedded in the bulk of electromagnetic shields fabricated in accordance with the improved technology reported herein allows one to deliver the required electromagnetic transmission coefficients and resonance frequencies of the shields. The smallest electromagnetic transmission coefficients for electromagnetic shields fabricated in accordance with the improved technology is achieved if the helical elements embedded in the bulk of the shields are arranged as shown in Fig. 2 *a* and *c*. Those electromagnetic shields show good promise for electronic de-

vice protection from electromagnetic noise with exactly known frequencies.

The electromagnetic transmission coefficients of the electromagnetic shields fabricated in accordance with the improved technology are comparable with the electromagnetic transmission coefficients of the electromagnetic shields fabricated in accordance with counterpart technologies [19–23, 25]. However the time consumption for the fabrication of shields in accordance with the improved technology is lower as compared to that for counterpart technologies [19–23, 25].

The introduction of sheet metallic materials in the bulk of electromagnetic shields fabricated in accordance with the improved technology (e.g. foiled metallic material sheets) provides structures exhibiting electromagnetic reflection coefficients of below  $-10.0$  dB due to the counter-phase interaction of electromagnetic waves reflected from helical elements embedded in the bulk of those structures and electromagnetic waves reflected from the surface of sheet metallic materials. The UHF electromagnetic transmission coefficient of these structures may reach  $-50.0$  dB due to the attenuation of electromagnetic radiation by the metallic material sheets embedded in the shield bulk. These structures show good promise for passive electromagnetic noise protection of electronic devices.

It should be noted that for the commercial fabrication of electromagnetic shields in accordance with the suggested improved technology, the helical elements for introduction in the bulk of the shields can be preferably fabricated by milling of foiled solid state materials (e.g. laminated fabric) on CNC milling machines.

One should also bear in mind is that the method of fusion bonding of radio-transparent synthetic unwoven fiber fabric which is the basis of the improved technology can be used for the fabrication of frequency-selective electromagnetic wire shields with embedded elements of other than helical shapes.

## References

1. Semenikhina D.V., Semenikhin A.I., Yukhanov Y.V. Effect of frequency selective shield of semielliptical shape on the characteristics of antenna array. *Proc. of Inter. conf. on computer information systems and industrial applications (CISIA 2015)*. June 28–29, 2015. Bangkok, Thailand. Atlantis Press; 2015. P. 107–109. <https://doi.org/10.2991/cisia-15.2015.28>
2. Singh A., Singh C. Quad-band FSS for electromagnetic shielding. *International Journal of Computer Communication and Informatics*. 2021; 3(1): 1–14. <https://doi.org/10.34256/ijcci2111>
3. Silva M.W.B., Junqueira C.C.M., Culhaoglu A.E., Kempfner E. Frequency selective smart shield design for wireless signals. *Proc. 9th European conf. on antennas and propagation (EuCAP2015)*. April 12–17, 2015. Lisbon, Portugal. <https://ieeexplore.ieee.org/document/7228738>
4. Koohestani M., Perdriau R., Ramdani M., Carlsson J. Frequency selective surfaces for electromagnetic shielding of pocket-sized transceivers. *IEEE Transactions on Electromagnetic Compatibility*. 2020; 62(6): 2785–2792. <https://doi.org/10.1109/temc.2020.2999635>
5. Konoplev I., Posthuma De Boer D.W., Warsop C., John M. Design and characterisation of frequency selective conductive materials for electromagnetic fields control. *Scientific Reports*. 2020; 10(1): 19351. <https://doi.org/10.1038/s41598-020-76447-x>
6. Mayouf A.T., Sayidmarie K.H., Mohammed Ali Y.E. A dual stopband frequency selective surface for mobile shielding applications. *IOP Conference Series: Materials Science and Engineering*. 2021; 1152(1): 012008. <https://doi.org/10.1088/1757-899X/1152/1/012008>
7. Khoshniat A., Abhari R. Suppression of radiated electromagnetic emissions using absorbing frequency selective surfaces. *2017 IEEE*

- 26th Conference on Electrical Performance of Electronic Packaging and Systems (EPEPS); 2017. P. 1–3. <https://doi.org/10.1109/EPEPS.2017.8329705>
8. Perotoni M.B., Andrade L.A., Junqueira C. Design, prototyping and measurement of a cascaded 6-GHz frequency selective surface array. *Journal of Aerospace Technology and Management*. 2016; 8(2): 137–142. <https://doi.org/10.5028/jatm.v8i2.629>
  9. Hussein M., Zhou J., Huang Y., Al-Juboori B. A low-profile miniaturized second-order bandpass frequency selective surface. *IEEE Antennas Wireless Propagation Letters*. 2017; 16: 2791–2794. <https://doi.org/10.1109/LAWP.2017.2746266>
  10. De Siqueira Campos A.L.P., Maniçoba R.H.C., d’Assunção A.G. Investigation of enhancement band using double screen frequency selective surfaces with Koch fractal geometry at millimeter wave range. *Journal of Infrared, Millimeter and Terahertz Waves*. 2010; 31(12): 1503–1511. <https://doi.org/10.1007/s10762-010-9735-8>
  11. Liu P., Yang S., Jain A., Wang Q., Jiang H., Song J., Koschny T., Soukoulis C.M., Dong L. Tunable meta-atom using liquid metal embedded in stretchable polymer. *Journal of Applied Physics*. 2015; 118(1): 014504–014902. <https://doi.org/10.1063/1.4926417>
  12. Yang S., Liu P., Yang M., Wang Q., Song J., Dong L. From flexible and stretchable meta-atom to metamaterial: A wearable micro-wave meta-skin with tunable frequency selective and cloaking effects. *Scientific Reports*. 2016; 6(1): 21921. <https://doi.org/10.1038/srep21921>
  13. Sessions D., Cook A., Fuchi K., Gillman A., Huff G., Buskoh P. Origami-inspired frequency selective surface with fixed frequency response under folding. *Sensors*. 2019; 19(21): 4808–4828. <https://doi.org/10.3390/s19214808>
  14. Perotoni M.B., Andrade L.A., Junqueira C. Design, prototyping and measurement of a cascaded 6-GHz frequency selective surface array. *Journal of Aerospace Technology and Management*. 2016; 8(2): 137–142. <https://doi.org/10.5028/jatm.v8i2.629>
  15. Liang B., Bai M. Subwavelength three-dimensional frequency selective surface based on surface wave tunneling. *Optics Express*. 2016; 24(13): 14697–14702. <https://doi.org/10.1364/OE.24.014697>
  16. Sanz-Izquierdo B., Parker E.A. 3D Printing technique for fabrication of frequency selective structures for built environment. *Electronics Letters*. 2013; 49(18): 1117–1118. <https://doi.org/10.1049/el.2013.2256>
  17. Novikova Yu.A. Overview of unmanaged and controllable frequency-selective surfaces. *The collection of reports of the 1st All-Russ. scient. conf. “Modeling and situational quality control of complex systems”*. April 14–22, 2020, St. Petersburg. St. Petersburg: Sankt-Peterburgskii gosudarstvennyi universitet aerokosmicheskogo priborostroeniya; 2020. P. 95–98. (In Russ.). <https://doi.org/10.31799/978-5-8088-1449-3-2020-1-95-98>
  18. Anwar R.S., Mao L., Ning H. Frequency selective surfaces: A review. *Applied Sciences*. 2018; 8(9): 1689–1736. <https://doi.org/10.3390/app8091689>
  19. Martinez-Lopez L., Rodriguez-Cuevas J., Martinez-Lopez J.I., Martynyuk A.E. A multilayer circular polarizer based on bisected split-ring frequency selective surfaces. *IEEE Antennas Wireless Propagation Letters*. 2014; 13: 153–156. <https://doi.org/10.1109/LAWP.2014.2298393>
  20. Campos A.L.P.; de Oliveira E.E.C.; da Fonseca Silva P.H. Design of miniaturized frequency selective surfaces using Minkowski island fractal. *Journal of Microwaves, Optoelectronics and Electromagnetic Applications (JMoe)*. 2010; 9(1): 43–49.
  21. Yao X., Bai M., Miao J. Equivalent circuit method for analyzing frequency selective surface with ring patch in oblique angles of incidence. *IEEE Antennas Wireless Propagation Letters*. 2011; 10: 820–823. <https://doi.org/10.1109/LAWP.2011.2164774>
  22. Li W., Wang C., Zhang Y., Li Y. A miniaturized frequency selective surface based on square loop aperture element. *International Journal Antennas Propagation*. 2014; 2014: 1–6. <https://doi.org/10.1155/2014/701279>
  23. Huang F.-C., Chiu C.-N., Wu T.-L., Chiou Y.-P. A circular-ring miniaturized-element metasurface with many good features for frequency selective shielding applications. *IEEE Transactions on Electromagnetic Compatibility*. 2015; 57(3): 365–374. <https://doi.org/10.1109/TEM.2015.2389855>
  24. Panwar R., Lee J.R. Progress in frequency selective surface-based smart electromagnetic structures: A critical review. *Aerospace Science and Technology*. 2017; 66: 216–234. <https://doi.org/10.1016/j.ast.2017.03.006>
  25. Liu T., Kim S.-S. High-capacitive frequency selective surfaces of folded spiral conductor arrays. *Microwave and Optical Technology Letter*. 2020; 62(1): 301–307. <https://doi.org/10.1002/mop.32006>
  26. Chena T.-K., Huff G.H. Transmission line analysis of the Archimedean spiral antenna in free space. *Journal of Electromagnetic Waves and Applications*. 2014; 28(10): 1175–1193. <https://doi.org/10.1080/09205071.2014.909295>